



38 Relative Humidity (RH) is a key meteorological parameter that determines the
39 aerodynamic component of the atmospheric evaporative demand (AED) (Wang and
40 Dickinson, 2012; McVicar et al., 2012a). As such, changes in RH may impact
41 significantly the evolution of the AED (Vicente-Serrano et al., 2014a), with particular
42 implications for the intensity of the hydrological cycle (Sherwood, 2010), climate
43 aridity (Sherwood and Fu, 2014) as well as severity of drought events (Rebetez et al.,
44 2006; Marengo et al., 2008).

45 In a changing climate, temperature rise, as suggested by different climate scenarios,
46 may impact the atmospheric humidity. According to the Classius-Clapeyron (CC)
47 relationship, a temperature rise of 1 °C is sufficient to increase the water holding
48 capacity of the air by roughly 7%. Given the unlimited water availability in the oceans
49 as well as the projected temperature rise, water vapor content could increase, at least in
50 the oceanic areas, in order to maintain RH constant in future. Particularly, there is an
51 empirical evidence on the increase in the water vapor content at both the surface and
52 upper tropospheric levels (Trenberth et al., 2005). In this context, numerous studies
53 have supported the constant RH scenario under global warming conditions (e.g. Dai,
54 2006; Lorenz and Deweaver 2007; Willett et al., 2008; McCarthy et al., 2009; Ferraro et
55 al., 2015). In contrast, other studies supported the non-stationary behavior of RH, not
56 only in continental areas located far from oceanic humidity (e.g. Pierce et al., 2013), but
57 also in humid regions (e.g. Van Wijngaarden and Vincent, 2004). Assuming the
58 stationary behavior of RH, the influence of RH on AED may be constrained, given that
59 any possible change in AED would be mostly determined by changes in other
60 aerodynamic variables (e.g. air temperature and wind speed) (McVicar et al., 2012a and
61 b) or by changes in cloudiness and solar radiation (Roderick and Farquhar, 2002; Fan
62 and Thomas, 2013). However, a range of studies have supported the non-stationary



63 behavior of RH under global warming, giving insights on significant changes in RH
64 over the past decades. A representative example is Simmons et al. (2010) who
65 compared gridded observational and reanalysis RH data, suggesting a clear dominant
66 negative trend in RH over the Northern Hemisphere since 2000. Also, based on a newly
67 developed homogeneous gridded database that employed the most available stations
68 from the telecommunication system of the WMO, Willett et al. (2014) found significant
69 negative changes in RH, with strong spatial variability, at the global scale. This global
70 pattern was also confirmed at the regional scale, but with different signs of change,
71 including both negative (e.g. Vincent et al., 2007; Vicente-Serrano et al., 2014b; 2016;
72 Zongxing et al., 2014) and positive trends (e.g. Shenbin, 2006; Jhajharia et al., 2009;
73 Hosseinzadeh Talaei et al., 2012).

74 There are different hypotheses that explain the non-stationary evolution of RH under
75 global warming conditions. One of these hypotheses is related to the slower warming of
76 oceans in comparison to continental areas (Lambert and Chiang, 2007; Joshi et al.,
77 2008). In particular, specific humidity of air advected from oceans to continents
78 increases more slowly than saturation specific humidity over land (Rowell and Jones
79 2006; Fasullo 2010). This would decrease RH over continental areas, inducing an
80 increase in AED and aridity conditions (Sherwood and Fu, 2014). Some studies
81 employed global climate models (GCMs) to support this hypothesis under future
82 warming conditions (e.g. Joshi et al., 2008; O’Gorman and Muller, 2010; Byrne and
83 O’Gorman, 2013). Nonetheless, there are unavailable empirical studies that support this
84 hypothesis using observational data. Moreover, the observed decrease in RH over some
85 coastal areas, which are adjacent to their sources of moisture, adds further uncertainty to
86 this hypothesis (Vicente-Serrano et al., 2014b and 2016; Willett et al., 2014).



87 Another hypothesis to explain the non-stationary evolution of RH under global warming
88 is associated with land-atmosphere feedback processes. Different studies indicated that
89 atmospheric moisture and precipitation are strongly linked to moisture recycling in
90 different regions of the world (e.g. Rodell et al., 2015). Thus, evapotranspiration may
91 contribute largely to water vapor content and precipitation over land (Stohl and James,
92 2005; Bosilovich and Chern, 2006; Trenberth et al., 2007; Dirmeyer et al., 2009; van
93 der Ent et al., 2010). Land-atmospheric feedbacks may also have marked influence on
94 atmospheric humidity (Seneviratne et al., 2006); given that soil drying can suppress
95 evapotranspiration, reduce RH and thus reinforce AED. All these processes would again
96 reinforce soil drying (Seneviratne et al., 2002; Berg et al., 2016).

97 Indeed, it is very difficult to determine which hypothesis can provide an understanding
98 of the observed RH trends at the global scale. Probably, the two hypotheses combined
99 together can be responsible for the observed RH trends in some regions of the world
100 (Rowell and Jones, 2006). In addition to the aforementioned hypotheses, some dynamic
101 forces, which are associated with atmospheric circulation processes, can explain the
102 non-stationary behavior of RH worldwide. Nonetheless, defining the relative
103 importance of these physical processes in different world regions is quite challengeable
104 (Zhang et al., 2013; Laua and Kim, 2015).

105 The objective of this study is to compare the recent variability and trends of RH with
106 changes in the two types of fluxes that affect RH: i) vertical fluxes that were assessed
107 using land evapotranspiration and precipitation and ii) advections that were quantified
108 using oceanic evaporation from moisture source areas. The novelty of this work stems
109 from the notion that although different studies have already employed GCM's and
110 different scenarios to explain the possible mechanisms behind RH changes under
111 warming conditions, we introduce a new empirical approach that employs different



112 observational data sets, reanalysis fields and a lagrangian-based approach, not only for
113 identifying the continental and oceanic moisture areas for different target regions, but
114 also for exploring the relevance of the existing hypothesis to assess the magnitude, sign
115 and spatial patterns of RH trends in the past decades at the global scale.

116

117 **2. Data and methods**

118 2.1. Data

119 *2.1.1. HadISDH data set*

120 We employed the monthly RH HadISDH dataset, available through
121 <http://www.metoffice.gov.uk/hadobs/hadisdh/>. This dataset represents the most
122 complete and accurate global dataset for RH, including observational data from a wide
123 range of stations worldwide (Willet et al., 2014). Given that HadISDH includes some
124 series with data gaps; our decision was to choose only those series with no more than
125 20% of missing values over the period 1979-2014. In order to fill these gaps, we created
126 a standardized regional series for each station using the most correlated series with each
127 target series. While this procedure maintains the temporal variance of the original data,
128 it provides a low biased estimation of the missing values. Overall, a final dataset of
129 3462 complete stations spanning different regions worldwide and covering the period
130 1979-2014 was employed in this work.

131

132 *2.1.2. ERA-Interim dataset*

133 Daily data of dewpoint (T_d), air temperature (T) and surface pressure (P_{mst}) at a spatial
134 interval of 0.5° was obtained from the ERA-Interim covering the period 1979-2014
135 (<http://www.ecmwf.int/en/research/climate-reanalysis/era-interim>) (Dee et al., 2011).

136 Based on the selected variables, we calculated the daily RH following Buck (1981):



137
$$RH = 100 \left(\frac{e}{e_s} \right) \quad (1)$$

138 where e is the actual vapor pressure and e_s is the saturated vapor pressure. As a function
139 of the wet bulb air temperature (T_w), e is estimated following two different equations
140 with respect to water/ice. If T_w is above 0°C , e is calculated as :

141
$$e = 6.1121 \cdot f_w \exp \left(\frac{\left(\frac{18.729 - \left[\frac{T_d}{227.31} \right]}{257.78 + T_d} \right) \cdot T_d}{257.78 + T_d} \right) \quad (2)$$

142 If T_w is below 0°C , e it is calculated as:

143
$$e = 6.1115 \cdot f_i \exp \left(\frac{\left(\frac{23.036 - \left[\frac{T_d}{333.7} \right]}{279.82 + T_d} \right) \cdot T_d}{279.82 + T_d} \right) \quad (3)$$

144 where

145
$$f_w = 1 + 7 \times 10^{-4} + 3.46 \times 10^{-6} P_{mst} \quad (4)$$

146
$$f_i = 1 + 3 \times 10^{-4} + 4.18 \times 10^{-6} P_{mst} \quad (5)$$

147 T_w is obtained according to Jensen et al. (1990):

148
$$T_w = \frac{aT + bT_d}{a + b} \quad (6), \text{ where}$$

149
$$a = 6.6 \times 10^{-5} P_{mst} \quad (7)$$

150
$$b = \frac{409.8e}{(T_d + 237.3)^2} \quad (8)$$

151 e_s is obtained by substituting T_d by T .

152 2.1.3. Land precipitation and land air temperature

153 We employed the gridded land precipitation and surface air temperature data (TS
154 v.3.23), provided by the Climate Research Unit (UK), at a 0.5° spatial interval for the
155 period 1979-2014 (Harris et al., 2014). This product was developed using a relatively
156 high number of observational sites, which guarantees a robust representation of climatic
157 conditions across worldwide regions. Importantly, this product has been carefully tested
158 for potential data inhomogenities as well as anomalous data.

159

160 2.1.4. Sea Surface Temperature (SST)



161 We used the monthly SST data (HadSST3), compiled by the Hadley Centre for the
162 common period 1979-2014 (<http://www.metoffice.gov.uk/hadobs/hadsst3/>). This dataset
163 is provided at a 0.5° grid interval (Kennedy et al., 2011a and b).

164

165 *2.1.5. Ocean evaporation and continental evapotranspiration data*

166 To quantify the temporal variability and trends of land evapotranspiration and oceanic
167 evaporation, we employed two different datasets. First, the oceanic evaporation was
168 quantified using the Objectively Analyzed air-sea Fluxes (OAFLUX) product (Yu et al.,
169 2008), which was used to analyze recent variability and changes in evaporation from
170 global oceans (Yu, 2007). To account for land evapotranspiration, we employed the
171 Global Land Evaporation Amsterdam Model (GLEAM) (Version 3.0a)
172 (<http://www.gleam.eu/>) (Miralles et al., 2011). This data set has been widely validated
173 using in situ measurements of surface soil moisture and evaporation across the globe
174 (Martens et al., 2016).

175

176 2.2. Methods

177 *2.2.1. Relative Humidity (RH) trends*

178 We assessed the seasonal (boreal cold season: October-March; boreal warm season:
179 April-September) and annual trends of RH for 1979-2014 using two different global
180 datasets (HadISDH and ERA-Interim). To quantify the magnitude of change in RH, we
181 used a linear regression analysis between the series of time (independent variable) and
182 RH series (dependent variable). The slope of the regression indicates the amount of
183 change (per year), with higher slope values indicating greater changes. To assess the
184 statistical significance of the detectable changes, we applied the nonparametric Mann–
185 Kendall statistic, which measures the degree to which a trend is consistently increasing
186 or decreasing (Zhang et al., 2001). To account for any possible influence of serial



187 autocorrelation on the robustness of the defined trends, we applied the modified Mann–
188 Kendall trend test, which returns the corrected p-values after accounting for temporal
189 pseudoreplication in RH series (Hamed and Rao, 1998; Yue and Wang, 2004). The
190 statistical significance of the time series was tested at the 95% confidence interval
191 ($p < 0.05$).

192 Following the trend analysis results, we selected those regions that showed a high
193 agreement between HadISDH and ERA-Interim datasets in terms of the sign and
194 magnitude of RH changes. Nonetheless, we also extended our selection to some other
195 regions, with uneven number of stations in the HadISDH dataset. This decision was
196 simply motivated by the consistent changes found over these regions, as suggested by
197 the ERA-Interim dataset. For all the defined regions, we identified the oceanic and
198 continental moisture sources by means of the FLEXPART lagrangian model.

199

200 *2.2.2. Identification of continental and oceanic moisture sources*

201 We used the FLEXPART V9.0 particle dispersion model fed with the ERA-Interim
202 reanalysis data. According to this model, the atmosphere is divided homogeneously into
203 three-dimensional finite elements (hereafter “particles”); each represents a fraction of
204 the total atmospheric mass (Stohl and James, 2004). These particles may be advected
205 backward or forward in time using three-dimensional wind taken from the ERA-Interim
206 data every time step, with superimposed stochastic turbulent and convective motions.
207 The rates of increase (e) and decrease (p) of moisture (e-p) along the trajectory of each
208 particle were calculated via changes in the specific moisture (q) with time ($e-p =$
209 mdq/dt), where m is the mass of the particle. Similar to the wind field, q is also taken
210 from the meteorological data. FLEXPART allows identifying the particles affecting a



211 particular region using information about the trajectories of these selected particles. A
212 description of this methodology is detailed in Stohl and James (2004).
213 The FLEXPART dataset used in this study was provided by a global experiment in
214 which the entire global atmosphere was divided into approximately 2.0 million
215 “particles”. The tracks were computed using the ERA-Interim reanalysis data at 6 h
216 intervals, at a 1° horizontal resolution and at a vertical resolution of 60 levels from 0.1
217 to 1000 hPa. For each particular target region, all the particles were tracked backward in
218 time, and its position and specific humidity (q) were recorded every 6 h. With this
219 methodology, the evaporative sources and sink regions for the particles reaching the
220 target region can be identified. All areas where the particles gained humidity ($E - P > 0$)
221 along their trajectories towards the target region can be considered as “sources of
222 moisture”. In contrast, all areas with lost humidity ($E - P < 0$) are considered as “sinks”.
223 A typical period used to track the particles backward in time is 10 days that is the
224 average residence time of water vapor in the global atmosphere (Numaguti, 1999).
225 However, we followed the methodology of Miralles et al (2016), where an optimal
226 lifetime of vapor in the atmosphere was calculated to reproduce as better as possible the
227 sources of moisture. As such, three steps were carried out in this order: i) all the
228 particles that leave each target region were tracked back during 10 days and the “initial
229 sources” at annual scale were defined as those areas with positive ($E - P$) values, ii) from
230 these “initial sources”, all the particles were forward tracked during 1 to 10 days
231 individually, and $(E - P) < 0$ was calculated for these lifetime periods to estimate the
232 precipitation contribution over the target region, iii) the optimal lifetime selected for
233 each region was that fulfills the minimum absolute difference between the FLEXPART
234 simulated precipitation and the CRU TS v.3.23 for each region, iv) and finally the
235 backward tracking was recalculated during these optimal lifetimes.



236 We defined the climatological spatial extent of each source region corresponding to a
237 particular target region by applying a 95th percentile criterion computed for the annual
238 and seasonal (boreal summer and winter) positive (E-P) field (Vazquez et al., 2016).
239 Then, for each year of the period, we estimated the total moisture support from each
240 source region.

241

242 *2.2.3. Relationship between RH and the selected land/oceanic climate variables*

243 Based on defining the spatial extent of each moisture source region, we calculated
244 annual, warm and cold season regional series for ocean evaporation and land
245 evapotranspiration using the OAFUX and GLEAM datasets, respectively. The
246 regional series of ocean evaporation and land evapotranspiration were created using a
247 weighted average based on the seasonal/annual fields of (E-P)>0 (Section 2.2.2). This
248 approach allows creating a time series that better represents the interannual variability
249 of ocean evaporation and land evapotranspiration in the source(s) of moisture for each
250 defined region. Following the same approach, we also calculated the regional series of
251 SST corresponding to each oceanic moisture source region. Likewise, we calculated the
252 regional series of land precipitation and air temperature for each target region using
253 CRU TS v.3.23 dataset, and the ratio between air temperature in the target region and
254 SST in the source region.

255 For each target region, we related the regional series of seasonal and annual RH with the
256 corresponding regional times series of all aforementioned climatic variables. However,
257 to limit the possible influence of the trends presented in the data itself on the computed
258 correlations, we de-trended the series of the climate variables prior to calculating the
259 correlation. We also assessed changes in the regional series of the different variables;
260 their statistical signification was tested by means of the modified Mann-Kendall test at



261 the 95% level. Here, we also computed the association between RH and land
262 evapotranspiration at the annual and seasonal scales using the available gridded
263 evapotranspiration series. While a pixel-to-pixel comparison does not produce a reliable
264 assessment of the possible contribution of land evapotranspiration to RH changes, given
265 that the source of moisture can apparently be far from the target region, we still believe
266 that this association can give insights on the global influence of land evapotranspiration
267 on RH changes.

268 For each target region, we summarized the results of the magnitude of change in RH as
269 well as other investigated variables at the seasonal and annual scales. However, to
270 facilitate the comparison among the different variables and the target regions
271 worldwide, we transformed the amount of change of each variable to percentages.

272

273 **3. Results**

274 **3.1. Trends in Relative Humidity**

275 Figure 1 summarizes the magnitude of change in RH for the boreal cold and warm
276 seasons and at the annual scale, calculated using the annual and seasonal (boreal
277 summer and winter) positive (E-P) field for the period between 1979 and 2014. For
278 HadISDH, it is noted that the available RH stations is unevenly distributed over the
279 globe, with higher density in the mid-latitudes of the Northern Hemisphere.
280 Nevertheless, the available stations show coherent and homogeneous spatial patterns of
281 RH changes. In the boreal cold season, the most marked decrease was observed in the
282 Southwest and areas of Northeast North America, central Argentina, the Fertile
283 Crescent region in western Asia, Kazakhstan, as well as in the eastern China and the
284 Korea Peninsula. On the contrary, dominant RH increase was recorded in larger areas,
285 including most of Canada (mostly in the Labrador Peninsula), and large areas of North
286 and central Europe and India. While the density of complete and homogeneous RH



287 series is low, we found a dominant positive trend across the western Sahel and South
288 Africa. The ERA-Interim dataset showed magnitudes of change close to those suggested
289 by HadISDH. In addition, the ERA-Interim also provides information on RH changes in
290 regions with uneven distribution of RH observations (e.g. East Amazonian, east Sahel
291 and Iran), suggesting a dominant RH decrease across these regions.

292 For the boreal warm season, a clear tendency towards a reduction in RH was observed
293 in vast regions of the world, including (mostly the Iberian Peninsula, France, Italy,
294 Turkey and Morocco), Eastern Europe, and western part of Russia. Based on the
295 available stations across central Asia, we also found a general reduction of RH; a
296 similar pattern was also observed in East Asia, including Mongolia, east China, north
297 Indonesia, south Japan and Korea. This reduction was also noted South America, with a
298 general homogeneous pattern over Peru, Bolivia and a strong decrease over central
299 Argentina. On the contrary, the positive evolution of RH observed during the cold
300 season across Canada and Scandinavia was reinforced during the boreal warm season.
301 In the west Sahel and India, we found an upward trend of RH. The ERA-Interim also
302 revealed a strong RH decrease over the whole Amazonian region and the West Sahel,
303 while a marked increase dominated over the Andean region between Colombia, Ecuador
304 and North Peru. In Australia, the spatial patterns were more complex than those
305 obtained using the available observatories.

306 The HadISDH dataset suggests a general decrease of RH over Southwest North
307 America, Argentina, central Asia, Turkey, Mongolia and China, with a particular
308 reduction over the East Sahel, Iran, Mongolia and the eastern Asia. On the contrary, a
309 dominant positive trend was observed across Canada, areas of North Southern America,
310 the western Sahel, South Africa (Namibia and Botswana), some areas of Kenya, India
311 and the majority of Australia. A wide range of these regions exhibited statistically



312 significant trends from 1979 to 2014. (Supplementary Figure 1). A statistically
313 significant negative trend was observed at the seasonal and annual scales, not only in
314 most of Southern America and Northern America, but in large regions of Africa, South
315 Europe, central and East Asia as well. On the contrary, areas of complex topography in
316 the Northern Hemisphere, Australia, India, Northern South America and Africa showed
317 positive trends.

318 Albeit with these complex spatial patterns of RH changes, there is a globally dominant
319 negative trend (Figure 2). This pattern was observed using both the HadISDH and the
320 ERA-Interim datasets, although there is marked spatial bias in data availability of the
321 HadISDH. Figure 3 illustrates the relationship between the magnitudes of change in
322 RH, as suggested by the HadISDH dataset versus the ERA-Interim dataset. At the
323 seasonal and annual scales, there is a relatively high correlation (mostly above 0.55).
324 Given this high consistency between the HadISDH and the ERA-Interim datasets in
325 terms of both the magnitude and sign of change of in RH (Supplementary Figures 2 and
326 3), we decided to restrict our subsequent analysis to the ERA-Interim dataset, recalling
327 its denser global coverage compared to the HadISDH.

328 As RH is mostly dependent on changes in specific humidity (q), there is a dominant
329 high correlation between the interannual variability of RH and q (Supplementary Figure
330 4). In accordance, the magnitude of observed change in these two variables showed a
331 strong agreement for 1979-2014. Figure 4 summarizes the magnitude of change in
332 specific humidity (q) as well as changes in specific humidity necessary to maintain RH
333 constant as recorded in 1979. Specific humidity showed the strongest decrease in
334 Southwest North America, the Amazonian region, Southern South America and the
335 Sahel regions: a spatial pattern that is similar to RH pattern. Given the evolution of air



336 temperature between for 1979-2014, these regions exhibited a deficit of water vapor on
337 the order of -2 g/kg^{-1} in order to maintain RH constant.

338

339 **3.2. Spatial patterns of the dependency between RH and climate variables**

340 Based on the high agreement between the HadISDH and the ERA-Interim datasets in
341 reproducing consistent seasonal and annual trends in RH, we selected a range of regions
342 (N=14) worldwide (Figure 5). For these selected regions, we assessed the connection
343 between RH and some relevant climatic variables for the period 1979-2014. In addition,
344 we defined the oceanic and continental sources of moisture corresponding to these
345 regions using the FLEXPART model. We assessed the optimal lifetime for each region:
346 during 4 days in back for regions 1-5 and 7-11, during 5 days for regions 6, 12-13, and
347 during 7 days for region 5 (see section 2.2).

348 Figures 6-8 show some examples of the dependency between RH and different climate
349 variables at the annual scale. Results for all regions at the seasonal and annual scales are
350 presented in supplementary materials. Figure 6 (top) illustrates RH trends in the West
351 Sahel using the HadISDH and ERA-Interim datasets. We also showed the distribution
352 of the average annual moisture sources (E-P in mm) over this region for 1979-2014. As
353 illustrated, the atmospheric moisture is mostly coming from the western Sahel region
354 itself, in addition to some oceanic sources located in the central eastern Atlantic Ocean.
355 At the seasonal scale, there are some differences in the location and the intensity of the
356 moisture sources, with more oceanic contribution during the boreal warm season.
357 Nonetheless, in both cases, the continental moisture seems to be the key source of
358 humidity in the region (Suppl. Figures 20 and 34). In other areas, e.g. the Western
359 European region (Suppl. Figures 16 and 30), we observed marked differences in the
360 location and the intensity of humidity sources between the boreal cold and warm



361 seasons. Figure 6 (central) shows different scatterplots summarizing the relationships
362 between the de-trended annual series of RH and those of relevant climate variables (e.g.
363 precipitation, air temperature and SST). As illustrated, the interannual variability of RH
364 in the region is strongly controlled by changes in the total annual precipitation and the
365 total annual land evapotranspiration in the continental source region. Specifically, the
366 correlation between the de-trended annual RH and precipitation and land
367 evapotranspiration is generally above 0.8 ($p < 0.05$). In contrast, RH shows negative
368 correlations with air temperature and SST ratio over the oceanic source. While the
369 correlation is statistically insignificant ($p > 0.05$), it suggests that higher differences
370 between air temperature and SST reinforce lower annual RH. At the seasonal scale, we
371 found similar patterns (Supplementary Figs. 20 and 34), with RH being highly
372 correlated with land evapotranspiration during the boreal cold and warm seasons.
373 Nevertheless, in the warm season, a significant negative correlation with air temperature
374 and SST ratio was observed. These relationships together would explain the observed
375 trend in RH, which showed an average significant increase of 2% per decade. This
376 pattern concurs with the significant increase in specific humidity (q) for 1979-2014; this
377 is probably related to the high increase in land evapotranspiration (19.5%, $p < 0.05$).
378 These results would suggest that RH has mostly changed over the West Sahel region, as
379 a consequence of changes in the continental humidity sources.

380 Figure 7 summarizes the same results, but for La Plata region (South America). Results
381 indicate a general decrease in RH at the annual and seasonal scales using both the
382 HadISDH observational data and the ERA-Interim dataset. As depicted, the main
383 humidity sources are located in the same region, combined with some other continental
384 neighbor areas over South America. A similar finding was also observed at the seasonal
385 scale (Supplementary Figs. 24 and 38). Similar to the West Sahel region, we found a



386 significant association between the interannual variations of RH and precipitation and
387 the land evapotranspiration in the continental source region. Similarly, we did not find
388 any significant correlation between RH changes and the interannual variability of the
389 oceanic evaporation in the oceanic source region as well as the ratio between air
390 temperature in the continental target region and SST in the oceanic source region.
391 Again, we found a negative correlation between RH and air temperature/SST ratio,
392 though being statistically insignificant at the annual scale ($p > 0.05$). In La Plata region,
393 we noted a strong decrease in RH (-6.21%/decade) for 1979-2014, which agrees well
394 with the strong decrease in absolute humidity. This region is strongly impacted by
395 continental atmospheric moisture sources, with a general decrease in precipitation and
396 land evapotranspiration during the analyzed period. Given the high control of these
397 variables on the interannual variability of RH, it is reasonable to consider that a
398 decrease in precipitation and soil water content would reduce water supply to the
399 atmosphere by means of evapotranspiration processes. This would reduce specific
400 humidity (q) and ultimately RH.

401 Results for Southwest North America are also illustrated in Figure 8. In accordance with
402 both previous studied examples (West Sahel and La Plata), this region also exhibited a
403 strong and positive relationship between the interannual variability of RH and
404 precipitation and land evapotranspiration. This pattern was also recorded for the boreal
405 warm and cold seasons (Supplementary Figures 27 and 41). In this region, we found a
406 strong negative trend of RH for 1979-2014, which concurs with the significant decrease
407 of absolute humidity. We noted a significant increase in air temperature, air temperature
408 and SST ratio, while a negative and statistically significant decrease in land
409 evapotranspiration in the continental sources of moisture was observed.



410 Other regions of the world (see Supplementary Material) also showed strong
411 dependency between the interannual variability of RH and that of land
412 evapotranspiration in the land moisture sources. Some examples include Western
413 Europe, Central-eastern Europe, Southeast Europe, Turkey, India and the east Sahel.
414 Nevertheless, the influence of land evapotranspiration was very different between the
415 boreal warm and cold seasons (e.g. Scandinavia, Central-east Europe and the
416 Amazonian region). In contrast, other regions showed a weak correlation between the
417 temporal variability of RH and land evapotranspiration in the moisture source region. A
418 representative example is China, which witnessed a strong decrease in RH for 1979-
419 2014. In this region, RH changes correlated significantly with annual precipitation only:
420 a variable that did not show significant changes from 1979 to 2014 (Supplementary Fig.
421 10). This annual pattern was also observed for the boreal cold and warm seasons
422 (Supplementary Figs. 22 and 36).

423 Nevertheless, although the interannual variability of land evapotranspiration in the land
424 moisture sources showed the highest correlation with RH variability in the majority of
425 the analyzed regions, air temperature/SST ratio in the oceanic moisture sources also
426 exhibited negative correlations with RH in particular regions, including West Sahel, La
427 Plata, West Coast of the USA, Central-eastern Europe, India, central North America and
428 the Amazonian region. This finding suggests that higher differences between air
429 temperature in the target area and SST in the oceanic moisture region would favor
430 decreased RH.

431 In summary, changes in RH were mostly associated with the observed changes in land
432 evapotranspiration across the selected regions (Figure 9). In contrast, annual changes in
433 RH did not correlate significantly with precipitation, air temperature/SST and oceanic



434 evaporation. For the boreal warm and cold seasons we found a similar pattern
435 (Supplementary Figs. 44 and 45).

436

437 **3.3. Global relationship between RH and land evapotranspiration**

438 Figure 10 depicts the relationship between RH and land evapotranspiration seasonally
439 and annually at the global scale. Results reveal strong positive and significant
440 correlations in large areas of the world. The strongest positive correlations were found
441 in Central, West and Southwest North America, Argentina, east Brazil, South Africa,
442 the Sahel, central Asia and the majority of Australia. Nevertheless, there are some
443 exceptions, including large areas of the Amazon, China, central Africa and the high
444 latitudes of the Northern Hemisphere, where the correlations were negative. In general,
445 the areas with positive and significant correlations between RH and land
446 evapotranspiration corresponded to those areas characterized by semiarid and arid
447 climate characteristics, combined with some humid areas (e.g. India and northwest
448 North America).

449 Overall, the global trends in land evapotranspiration were spatially coherent with those
450 observed for RH. Figure 11 illustrates the spatial distribution of the magnitude of
451 change in annual and seasonal land evapotranspiration at the global scale from 1979 to
452 2014. As depicted, the spatial patterns of land evapotranspiration changes resemble
453 those of RH (refer to Figure 1). For example, a positive trend in the annual land
454 evapotranspiration dominated over the Canadian region, which agrees well with the
455 general increase in RH across the region. On the contrary, there was a dominant
456 decrease in the annual land evapotranspiration across vast areas of North America,
457 which concurs also with the strong decrease in RH. Similar to the pattern observed for
458 land evapotranspiration, RH increased particularly over southwest North America. In



459 South America, both variables also showed a dominant negative trend at the annual
460 scale, but with some spatial divergences, mainly in the Amazonian region. Specifically,
461 the western part of the basin showed the most important decrease in land
462 evapotranspiration, whereas the most significant decrease in RH was observed in the
463 eastern part. In the African continent, some areas showed good agreement between RH
464 and land evapotranspiration changes, in terms of both the sign and magnitude. This can
465 be clearly seen in the West and East Sahel, where a strong gradient in RH trend between
466 the West (positive) and the East (negative) was observed. A similar pattern was also
467 observed for the Namibia-Botswana-Angola region. Nevertheless, other African regions
468 showed a divergent pattern between both variables. One example is the Guinea Gulf in
469 Nigeria and Cameroon, where we noted a strong increase in land evapotranspiration, as
470 opposed to RH changes. In Australia, although both variables showed a dominant
471 positive trend, they did not match exactly in terms of the spatial pattern of the
472 magnitude of change. This is particularly because the main increase in RH was found in
473 the south, while the main increase in land evapotranspiration was noted in the north of
474 the Island. The Eurasian continent showed the main divergences between both
475 variables. In the high latitudes of the continent, there was a dominant increase in both
476 variables. For other regions (e.g. Western Europe), we noted a dominant RH decrease,
477 which was not observed for land evapotranspiration. A similar pattern was observed
478 over east China, with a dominant RH negative trend and a positive land
479 evapotranspiration.

480 Our results confirm that the global connection between oceanic evaporation and
481 changes in RH is complex. On one hand, it is difficult to establish a pixel per pixel
482 relationship. On the other hand, it is not feasible to identify moisture sources for each
483 0.5° pixel at the global scale. However, we believe that the analysis of the evolution of



484 SST and oceanic evaporation for 1979-2014 can give indications on some relevant
485 patterns. Figure 12 illustrates the spatial distribution of the magnitude of change of
486 annual and seasonal SST and oceanic evaporation. Supplementary Fig. 46 shows the
487 spatial distribution of trend significance. As depicted, complex spatial patterns and high
488 variability of the trends were observed, particularly for oceanic evaporation.
489 Furthermore, the spatial distribution of the magnitude of change in annual and seasonal
490 oceanic evaporation was not related to the SST changes (Supplementary Fig. 47). This
491 finding suggests that oceanic evaporation is not only driven by changes in SST. Thus,
492 although some regions showed positive changes in the oceanic evaporation, the amount
493 of increase was much lower than that found for SST, suggesting a general positive trend
494 in most of the world's oceans (Supplementary Figure 48, Supplementary Table 1).

495

496 **4. Discussion and conclusions**

497 We assessed the temporal variability and trends of relative humidity (RH) at the global
498 scale using a dense observational network of meteorological stations (HadISDH) and
499 reanalysis data (ERA-Interim). Results revealed high agreement of the interannual
500 variability of RH using both datasets for 1979-2014. This finding was also confirmed,
501 even for the regions where the density of the HadISDH observatories was quite poor
502 (e.g. the northern latitudes and tropical and equatorial regions). Recent studies have
503 suggested dominant decrease in observed RH during the last decade (e.g. Simmons et
504 al., 2010; Willet et al., 2014). Our study suggests dominant negative trends of RH using
505 the HadISDH dataset. This decrease is mostly linked to the temporal evolution of RH
506 during the boreal warm season. Nevertheless, other regions showed positive RH trends.
507 In accordance with the HadISDH dataset, the ERA-Interim revealed dominant negative
508 RH trends, albeit with a lower percentage of the total land surface compared to the



509 HadISDH dataset. These differences cannot be attributed to the selected datasets, given
510 that both mostly agree on the magnitude and sign of changes in RH.

511 Observed changes in RH were closely related to the magnitude and the spatial patterns
512 of specific humidity changes. Results demonstrate a general deficit of specific humidity
513 to maintain RH constant in large areas of the world, including the central and south
514 Northern America, the Amazonas and La Plata basins in South America and the East
515 Sahel. In other regions, RH increased in accordance with higher specific humidity.
516 Some studies suggested that changes in air temperature could partly cancel the effects of
517 the atmospheric humidity to explain RH changes (e.g. McCarthy and Tuomi, 2004;
518 Wright et al., 2010; Sherwood, 2010). Nevertheless, although air temperature trends
519 showed spatial differences at the global scale over the past four decades (IPCC, 2013),
520 our results confirm that air temperature is not the main driver of the observed changes
521 of RH globally. The ERA-Interim dataset clearly showed a close resemblance between
522 RH and specific humidity trends at the global scale. This suggests that specific humidity
523 is the main driver of the observed changes in the magnitude and spatial pattern of RH
524 during the past decades.

525 Overall, there is a strong agreement between the interannual variability of precipitation
526 and land evapotranspiration in the continental moisture source and the interannual
527 variability of RH in the different regions. Moreover, we found a close spatial
528 relationship between RH changes over each of these regions and the observed changes
529 in land evapotranspiration over the continental source regions. These findings suggest
530 that, at the annual and seasonal scales, the interannual variability of land
531 evapotranspiration was significantly correlated with RH changes over most of the
532 continental areas. Nonetheless, this finding should be seen in the context that RH at
533 each site cannot be determined only by the land/water supply from the site itself, but it



534 can further be controlled by land evapotranspiration over remote continental areas. This
535 finding highlights the importance of land evapotranspiration processes in defining RH
536 variability over large world areas.

537 In general, our results give additional support to the existing hypothesis of the strong
538 influence of land-atmosphere water feedbacks and recycling processes on RH variability
539 and trends. This is simply because more available soil humidity under favorable
540 atmospheric and land conditions would result in more evapotranspiration and
541 accordingly higher air moisture (Eltahir and Bras, 1996; Domínguez et al., 2006;
542 Kunstmann and Jung, 2007). Recalling that the ocean surface evaporates about 84% of
543 the water evaporated over the Earth (Oki, 2005), the oceanic evaporation is highly
544 important for continental precipitation (Gimeno et al., 2010). However, the continental
545 humidity sources can also be important. Numerous model-based studies have supported
546 the strong influence of land evaporation processes on air humidity and precipitation
547 over land surfaces (e.g. Bosilovich and Chern, 2006; Dirmeyer et al., 2009). Moisture
548 recycling is strongly important in some regions of the world, such as China and central
549 Asia, the western part of Africa and the central South America (Pfahl et al., 2014; van
550 der Ent et al., 2010). In Europe, Ruosteenoja and Raisanen (2013) linked RH variability
551 to some meteorological variables (e.g. air temperature, precipitation) in the Coupled
552 Model Intercomparison Project Phase 3 (CMIP3) models. They indicated that seasons
553 with anomalously large precipitation, which supply moisture to soils, are likely to
554 coincide with anomalous RH, particularly in Northern Europe. They also concluded that
555 an earlier springtime drying of soil in future will suppress evapotranspiration and
556 further reduce RH over land. Similarly, Rowell and Jones (2006) analyzed different
557 hypotheses to explain the projected summer drying conditions in Europe, suggesting
558 that soil moisture decline and land–sea contrast in lower tropospheric summer could be



559 the key factors responsible for this drying. They concluded that reduced evaporation in
560 summer will drop RH and hence reduced continental rainfall. These would impact soil
561 moisture and evapotranspiration processes, inducing a reduction in RH and rainfall,
562 through a range of atmospheric feedbacks. In the same context, the importance of
563 moisture recycling processes for atmospheric humidity and precipitation has been
564 recently identified in semi-arid and desert areas of the world (Miralles et al., 2016).

565 Although our study was limited to specific regions across the world, results indicate that
566 humidity in the analyzed regions is largely originated over continental rather than
567 oceanic areas. This finding concurs with some regional studies that defined sources of
568 moisture (e.g., Nieto et al., 2014; Gimeno et al., 2010; Drumond et al., 2014; Ciric et al.,
569 2016). Also, our results suggest a strong association between land evapotranspiration
570 and RH variability, stressing the high importance of humidity recycling processes for
571 explaining RH variability over continental areas.

572 In contrast to the general high correlations found between the interannual variability of
573 RH and land evaporation, the ratio between air temperature and SST in the source
574 region did not show significant correlations with RH changes, albeit with the dominant
575 positive trend found for this ratio in the majority of the analyzed regions. Different
576 modelled climate studies suggested strong differences between land and ocean RH
577 trends, as a consequence of the different warming rates between oceanic and continental
578 areas (e.g. Joshi et al., 2008; Dessler and Sherwood, 2009; O’Gorman and Muller,
579 2010). As the warming rates are generally slower over oceans, the specific humidity of
580 air advected from oceans to continents would increase more slowly than the saturation
581 specific humidity over land, causing a reduction in RH (Rowell and Jones 2006). Due to
582 this effect, RH will not remain constant in areas located very far from humidity sources,
583 as warmer air temperatures under limited moisture humidity would reduce RH (Pierce et



584 al., 2013). Recalling the observed negative RH trend at many coastal regions over the
585 period 1979-2014, this study confirms that the distance to oceanic humidity sources is
586 not a key controller of the spatial patterns of RH changes.. In many instances, we found
587 that continental regions, which are very far from oceans (e.g. Canada, central China and
588 Kazakhstan), recorded a positive RH trend. This finding indicates that while different
589 model experiments fully supported the hypothesis that the different warming rates
590 between oceanic and continental areas can explain the projected decrease in RH under
591 climate change conditions, our results for 14 different regions in the world are
592 contradictory, given that most of these regions exhibited a negative RH trend for 1979-
593 2014. A possible explanation of these contrasting findings is related to the low
594 differences in the warming rates between the oceanic sources and continental target
595 areas. We found that -in most of the cases- these differences were not strong enough to
596 generate a clear effect at the global scale, particularly with the available number of
597 observations. The dominant negative correlation between RH and air temperature/SST
598 in the analyzed regions, though being weak, seems to support this finding.

599 Also, we did not find a significant relationship between the interannual variability of the
600 oceanic evaporation in the oceanic humidity source regions and RH in the target areas,
601 both at annual and seasonal scales. Although oceanic evaporation is decisive on
602 continental evaporation (Gimeno et al., 2010), current trends in RH are not related to the
603 observed oceanic evaporation trends over the humidity source areas. In accordance with
604 previous studies (e.g. Rayner et al., 2003; Deser et al., 2010), we found a general SST
605 increase in the oceanic areas at the global scale, albeit with some spatial exceptions.
606 Nevertheless, this increase does not imply that oceanic evaporation increased at the
607 same rate as SST. Here, we indicated that oceanic evaporation trends for 1979-2014
608 showed strong spatial variability at the global scale, with dominant positive trends.



609 Nonetheless, large areas also exhibited insignificant trends and even negative
610 evaporation trends. While SST increase is mainly associated with radiative processes,
611 evaporation processes are mainly controlled by a wide range of meteorological variables
612 that impact the aerodynamic and radiative components of the atmospheric evaporative
613 demand (AED) rather than SST alone (McVicar et al., 2012b). Due to the unlimited
614 water availability over oceans, air vapor pressure deficit is expected to be driven by the
615 Clausius-Clapeyron relation. However, changes in solar radiation and wind speed can
616 also influence the evaporation evolution (Yu, 2007; Kanemaru and Masunaga, 2013).
617 As such, given the slow oceanic evaporation trends in large regions of the world, RH
618 trends in the analyzed target regions can significantly be associated with oceanic
619 evaporation. Nevertheless, changes in other variables could also explain the relatively
620 small role of the oceanic moisture sources in RH variability and trends in the analyzed
621 continental areas. In this work, we did not consider the “effectivity” of the oceanic
622 moisture (Gimeno et al., 2012), since water vapor evaporated over the oceanic regions
623 could not reach the target region due to some geographical constraints (e.g.
624 topography). Also, we did not analyze the transport mechanisms between the source and
625 target areas. Moreover, moisture source regions are not stationary, as the intensity of
626 humidity can vary greatly from one year to another (Gimeno et al., 2013). This aspect
627 could be another source of uncertainty in the explanatory factors of current RH trends.
628 Furthermore, other different factors that control atmospheric humidity and RH have not
629 been approached in this study. Sherwood (1996) suggested that RH distributions are
630 strongly controlled by dynamical fields rather than local air temperatures. This suggests
631 that atmospheric circulation processes could largely affect the temporal variability and
632 trends of RH. A range of studies indicates noticeable changes in RH, in response to low-
633 frequency atmospheric oscillations, such as the Atlantic Multidecadal Oscillation



634 (AMO) and El Niño-Southern Oscillation (e.g. McCarthy and Toumi, 2004; Zhang et
635 al., 2013), as well as changes in the Hadley Circulation (HC) (Hu and Fu, 2007). Wright
636 et al. (2010) employed a global climate model under double CO₂ concentrations to show
637 that tropical and subtropical RH is largely dependent on a poleward expansion of the
638 Hadley cell: a deepening of the height of convective detrainment, a poleward shift of the
639 extratropical jets, and an increase in the height of the tropopause. Also, Laua and Kim
640 (2015) assessed changes in the HC under CO₂ warming from the Coupled Model
641 Intercomparison Project Phase-5 (CMIP5 model projections. They suggest that
642 strengthening of the HC induces atmospheric moisture divergence and reduces
643 tropospheric RH in the tropics and subtropics. This spatial pattern resembles the main
644 areas showing negative trends in RH in our analysis.

645 Considering all these limitations, we believe that further research is still needed to
646 consider other dynamic and radiative factors that may affect the temporal variability and
647 trends of RH over continental regions. Here, we found that actual evapotranspiration
648 processes from the continental humidity sources can impact recent temporal variability
649 and trends of RH. Overall, the proposed mechanisms by Sherwood and Fu (2014) of
650 increased aridity by enhanced AED driven by lower RH under a climate change
651 scenario is fully valid, regardless of which factors cause the reduction of RH.
652 Seneviratne et al. (2002) used a regional climate model, combined with a land-surface
653 scheme of intermediate complexity, to investigate the sensitivity of summer climate to
654 enhanced greenhouse warming over the American Midwest. They indicated that
655 vegetation control on transpiration might play an important part in counteracting an
656 enhancement of summer drying, particularly when soil water gets limited. Other studies
657 provide similar results in other regions using both observational data (e.g. Hisrchi et al.,
658 2011) and model outputs (e.g. Seneviratne et al., 2006; Fischer et al., 2007). Therefore,



659 the aridification processes would be even more severe if the suppression of the land
660 evapotranspiration is the main driver of RH reduction. Also, the AED can increase,
661 particularly when enhanced air dryness is driven by soil moisture dryness, inducing an
662 increase in aridity and the severity of drought episodes.

663

664 **Acknowledgements**

665 This work was supported by the EPhysLab (UVIGO-CSIC Associated Unit), PCIN-
666 2015-220, CGL2014-52135-C03-01, CGL2014-60849-JIN, *Red de variabilidad y*
667 *cambio climático* RECLIM (CGL2014-517221-REDT) financed by the Spanish
668 Commission of Science and Technology and FEDER, and IMDROFLOOD financed by
669 the Water Works 2014 co-funded call of the European Commission.

670

671 **References**

- 672 Berg, A., Findell, K., Lintner, B., et al.: Land-atmosphere feedbacks amplify aridity
673 increase over land under global warming, *Nature Climate Change*, 6, 869-874,
674 2016.
- 675 Bosilovich, M.G., Chern, J.-D.: Simulation of water sources and precipitation recycling
676 for the MacKenzie, Mississippi, and Amazon River basins, *Journal of*
677 *Hydrometeorology*, 7, 312-329, 2006.
- 678 Byrne, M.P., O’Gorman, P.A.: Link between land-ocean warming contrasts and surface
679 relative humidities in simulations with coupled climate models, *Geophysical*
680 *Research Letters*, 40, 5223-5227, 2013.
- 681 Buck, A. L.: New equations for computing vapor pressure and enhancement factor, *J.*
682 *Appl. Meteorol.*, 20, 1527–1532, 1981.
- 683 Ciric, D., Stojanovic, M., Drumond, A., Nieto, R., Gimeno, L.: Tracking the origin of
684 moisture over the danube river basin using a Lagrangian approach. *Atmosphere*,
685 7, 162, 2016.
- 686 Dai, A.: Recent climatology, variability, and trends in global surface humidity. *J Clim*,
687 19, 3589–3606, 2006.
- 688 Dee, D. P., Uppala, S. M., Simmons, A. J. et al.: The ERA-Interim reanalysis:
689 configuration and performance of the data assimilation system, *Q. J. R.*
690 *Meteorol. Soc.*, 137, 553–597, 2011.
- 691 Deser, C., Phillips, A.S., Alexander, M.A.: Twentieth century tropical sea surface
692 temperature trends revisited, *Geophysical Research Letters*, 37, L10701, 2010.
- 693 Dessler, A. E., Sherwood, S. C.: Atmospheric Science: A Matter of Humidity, *Science*,
694 323, 1020–1021, 2009.
- 695 Dirmeyer, P.A., Schlosser, C.A., Brubaker, K.L.: Precipitation, recycling, and land
696 memory: An integrated analysis, *Journal of Hydrometeorology*, 10, 278-288,
697 2009.
- 698 Dominguez, F., Kumar, P. Liang, X., Ting, M.: Impact of atmospheric moisture storage
699 on precipitation recycling, *J. Clim.*, 19, 1513–1530, 2006.



- 700 Drumond, A., Marengo, J., Ambrizzi, T. et al.: The role of the Amazon Basin moisture
701 in the atmospheric branch of the hydrological cycle: A Lagrangian analysis,
702 *Hydrology and Earth System Sciences*, 18, 2577-2598, 2014.
- 703 Eltahir, E.A.B., Bras, R.L.: Precipitation recycling, *Reviews of Geophysics*, 34, 367-
704 378, 1996.
- 705 Fan, Z.-X., Thomas, A.: Spatiotemporal variability of reference evapotranspiration and
706 its contributing climatic factors in Yunnan Province, SW China, 1961-2004,
707 *Climatic Change*, 116, 309-325, 2013.
- 708 Ferraro, A.J., Lambert, F.H., Collins, M., Miles, G.M.: Physical mechanisms of tropical
709 climate feedbacks investigated using temperature and moisture trends. *Journal of*
710 *Climate*, 28, 8968-8987, 2015.
- 711 Fischer, E.M., Seneviratne, S.I., Vidale, P.L., Lüthi, D., Schär, C.: Soil moisture-
712 atmosphere interactions during the 2003 European summer heat wave, *Journal of*
713 *Climate*, 20, 5081-5099, 2007.
- 714 Gimeno, L., Nieto, R., Trigo, R.M., Vicente-Serrano, S.M., López-Moreno, J.I.: Where
715 does the Iberian Peninsula moisture come from? An answer based on a
716 Lagrangian approach, *Journal of Hydrometeorology*, 11, 421-436, 2010.
- 717 Gimeno, L., Stohl, A., Trigo, R.M., et al.: Oceanic and terrestrial sources of continental
718 precipitation, *Reviews of Geophysics*, 50, RG4003, 2012.
- 719 Gimeno, L., Nieto, R., Drumond, A., Castillo, R., Trigo, R.: Influence of the
720 intensification of the major oceanic moisture sources on continental
721 precipitation, *Geophysical Research Letters*, 40, 1443-1450, 2013.
- 722 Hamed, K. H., Rao, A. R.: A modified Mann Kendall trend test for autocorrelated data,
723 *J. Hydrol.*, 204, 182–196, 1998.
- 724 Harris, I., Jones, P.D., Osborn, T.J., Lister, D.H.: Updated high-resolution grids of
725 monthly climatic observations – the CRU TS3.10 Dataset, *International Journal*
726 *of Climatology*, 34, 623–642, 2014.
- 727 Hirschi, M., Seneviratne, S.I., Alexandrov, V. et al.: Observational evidence for soil-
728 moisture impact on hot extremes in southeastern Europe, *Nature Geoscience*, 4,
729 17-21, 2011.
- 730 Hosseinzadeh Talaei, P., Sabziparvar, A.A., Tabari, H.: Observed changes in relative
731 humidity and dew point temperature in coastal regions of Iran, *Theoretical and*
732 *Applied Climatology*, 110, 385-393, 2012.
- 733 Hu, Y., Fu, Q.: Observed poleward expansion of the Hadley circulation since 1979,
734 *Atmospheric Chemistry and Physics*, 7, 5229-5236, 2007.
- 735 IPCC: Climate Change 2013: The Physical Science Basis. Contribution of Working
736 Group I to the Fifth Assessment Report of the Intergovernmental Panel on
737 Climate Change [Stocker, T.F., D. Qin, G.-K. Plattner, M. Tignor, S.K. Allen, J.
738 Boschung, A. Nauels, Y. Xia, V. Bex and P.M. Midgley (eds.)]. Cambridge
739 University Press, Cambridge, United Kingdom and New York, NY, USA, 1535
740 pp, 2013.
- 741 Jensen, M. E., Burman, R. D., and Allen, R. G. (Eds.): *Evapotranspiration and Irrigation*
742 *Water Requirements: ASCE Manuals and Reports on Engineering Practices No.*
743 *70*, American Society of Civil Engineers, New York, 360 pp., 1990.
- 744 Jhahharia, D., Shrivastava, S.K., Sarkar, D., Sarkar, S.: Temporal characteristics of pan
745 evaporation trends under the humid conditions of northeast India, *Agricultural*
746 *and Forest Meteorology*, 149, 763-770, 2009.
- 747 Joshi, M.M., Gregory, J.M., Webb, M.J., Sexton, D.M.H., Johns, T.C.: Mechanisms for
748 the land/sea warming contrast exhibited by simulations of climate change,
749 *Climate Dynamics*, 30, 455-465, 2008.



- 750 Kanemaru, K., Masunaga, H.: A satellite study of the relationship between sea surface
751 temperature and column water vapor over tropical and subtropical oceans,
752 *Journal of Climate*, 26, 4204-4218, 2013.
- 753 Kennedy J.J., Rayner, N.A., Smith, R.O., Saunby, M., Parker, D.E.: Reassessing biases
754 and other uncertainties in sea-surface temperature observations since 1850 part
755 1: measurement and sampling errors, *J. Geophys. Res.*, 116, D14103, 2011a.
- 756 Kennedy J.J., Rayner, N.A., Smith, R.O., Saunby, M. and Parker, D.E.: Reassessing
757 biases and other uncertainties in sea-surface temperature observations since 1850
758 part 2: biases and homogenisation. *J. Geophys. Res.*, 116, D14104, 2011b.
- 759 Kunstmann, H., Jung, G.: Influence of soil-moisture and land use change on
760 precipitation in the volta basin of West Africa, *International Journal of River
761 Basin Management*, 5, 9-16, 2007.
- 762 Lambert, F. H., Chiang, J.C.H.: Control of land-ocean temperature contrast by ocean
763 heat uptake, *Geophys. Res. Lett.*, 34, L13704, 2007.
- 764 Laua, W.K.M., Kim, K.-M.: Robust Hadley circulation changes and increasing global
765 dryness due to CO₂ warming from CMIP5 model projections. *Proceedings of
766 the National Academy of Sciences of the United States of America*, 112, 3630-
767 3635, 2015.
- 768 Lorenz, D.J., DeWeaver, E.T.: The response of the extratropical hydrological cycle to
769 global warming, *Journal of Climate*, 20, 3470-3484, 2007.
- 770 Marengo, J.A., Nobre, C.A., Tomasella, J. et al.: The drought of Amazonia in 2005,
771 *Journal of Climate*, 21, 495-516, 2008.
- 772 Martens, B., Miralles, D.G., Lievens, H., van der Schalie, R., de Jeu, R.A.M.,
773 Fernández-Prieto, D., Beck, H.E., Dorigo, W.A., and Verhoest, N.E.C.: GLEAM
774 v3: satellite-based land evaporation and root-zone soil moisture, *Geoscientific
775 Model Development Discussions*,
- 776 McCarthy, M.P., Toumi, R.: Observed interannual variability of tropical troposphere
777 relative humidity, *Journal of Climate*, 17, 3181-3191, 2004.
- 778 McCarthy, M.P., Thorne, P.W., Titchner, H.A.: An analysis of tropospheric humidity
779 trends from radiosondes, *Journal of Climate*, 22, 5820-5838, 2009.
- 780 McVicar, T.R., Roderick, M.L., Donohue, R.J., Van Niel, T.G.: Less bluster ahead?
781 Ecohydrological implications of global trends of terrestrial near-surface wind
782 speeds, *Ecohydrology*, 5, 381-388, 2012a.
- 783 McVicar, T.R., Roderick, M.L., Donohue, R.J., et al.: Global review and synthesis of
784 trends in observed terrestrial near-surface wind speeds: implications for
785 evaporation, *J. Hydrol*, 416-417, 182-205, 2012b.
- 786 Miralles, D.G., Holmes, T.R.H., de Jeu, R.A.M., Gash, J.H., Meesters, A.G.C.A.,
787 Dolman, A.J.: Global land-surface evaporation estimated from satellite-based
788 observations, *Hydrology and Earth System Sciences*, 15, 453-469, 2011.
- 789 Miralles, D.G., Nieto, R., McDowell, N.G., Dorigo, W.A., Verhoest, N.E.C., Liu, Y.Y.,
790 Teuling, A.J., Dolman, A.J., Good, S.P., Gimeno, L.: Contribution of water-
791 limited ecoregions to their own supply of rainfall, *Environmental Research
792 Letters*, 11, 124007, 2016.
- 793 Nieto, R., Castillo, R., Drumond, A., Gimeno, L.: A catalog of moisture sources for
794 continental climatic regions, *Water Resources Research*, 50, 5322-5328, 2014.
- 795 Numaguti, A.: Origin and recycling processes of precipitating water over the Eurasian
796 continent: experiments using an atmospheric general circulation model. *J.
797 Geophys. Res. Atmos.*, 104, 1957-1972, 1999.



- 798 O'Gorman, P.A., Muller, C.J.: How closely do changes in surface and column water
799 vapor follow Clausius-Clapeyron scaling in climate change simulations?
800 Environmental Research Letters, 5, 025207, 2010.
- 801 Oki, T.: The hydrologic cycles and global circulation. Encyclopedia of Hydrological
802 Sciences, 13-22. 2005.
- 803 Pfahl, S., Madonna, E., Boettcher, M., Joos, H., Wernli, H.: Warm conveyor belts in the
804 ERA-Interim Dataset (1979-2010). Part II: Moisture origin and relevance for
805 precipitation, Journal of Climate, 27, 27-40, 2014.
- 806 Pierce, D.W., Westerling, A.L., Oyler, J.: Future humidity trends over the western
807 United States in the CMIP5 global climate models and variable infiltration
808 capacity hydrological modeling system. Hydrology and Earth System Sciences,
809 17, 1833-1850, 2013.
- 810 Rayner, N.A., Parker, D.E., Horton, E.B. et al.: Global analyses of sea surface
811 temperature, sea ice, and night marine air temperature since the late nineteenth
812 century. Journal of Geophysical Research D: Atmospheres, 108, ACL 2-1 - ACL
813 2-29, 2003.
- 814 Rebetez, M., Mayer, H., Dupont, O., et al.: Heat and drought 2003 in Europe: A
815 climate synthesis, Annals of Forest Science, 63, 569-577, 2006.
- 816 Rodell, M., Beaudoin, H.K., L'Ecuyer, T.S. et al.: The observed state of the water
817 cycle in the early twenty-first century, Journal of Climate, 28, 8289-8318,
818 2015.
- 819 Roderick, M., Farquhar, G.D.: The cause of decreased pan evaporation over the past 50
820 years. Science, 15, 1410-1411, 2002.
- 821 Rowell, D.P., Jones, R.G.: Causes and uncertainty of future summer drying over
822 Europe, Climate Dynamics, 27, 281-299, 2006.
- 823 Ruosteenoja, K., Raisanen, P.: Seasonal changes in solar radiation and relative humidity
824 in europe in response to global warming, Journal of Climate, 26, 2467-2481,
825 2013.
- 826 Seneviratne, S.I., Pal, J.S., Eltahir, E.A.B., Schar, C.: Summer dryness in a warmer
827 climate: A process study with a regional climate model, Climate Dynamics, 20,
828 69-85, 2002.
- 829 Seneviratne, S.I., Lüthi, D., Litschi, M., Schär, C.: Land-atmosphere coupling and
830 climate change in Europe, Nature, 443, 205-209, 2006.
- 831 Shenbin, C., Yunfeng, L., Thomas, A.: Climatic change on the Tibetan Plateau:
832 Potential evapotranspiration trends from 1961-2000, Climatic Change, 76, 291-
833 319, 2006.
- 834 Sherwood, S.C.: Maintenance of the free-tropospheric tropical water vapor distribution.
835 Part I: Clear regime budget, Journal of Climate, 9, 2903-2918, 1996.
- 836 Sherwood, S.C.: Direct versus indirect effects of tropospheric humidity changes on the
837 hydrologic cycle, Environmental Research Letters, 5, 025206, 2010.
- 838 Sherwood, S., Fu, Q.: A drier future?, Science, 343, 737-739, 2014.
- 839 Simmons, A.J., Willett, K.M., Jones, P.D., Thorne, P.W., Dee, D.P.: Low-frequency
840 variations in surface atmospheric humidity, temperature, and precipitation:
841 inferences from reanalyses and monthly gridded observational data sets. J.
842 Geophys. Res .D Atmos., 115, D01110, 2010.
- 843 Stohl, A. and James, P.: A Lagrangian Analysis of the Atmospheric Branch of the
844 GlobalWaterWater Cycle. Part I: Method Description, Validation and
845 Demonstration for the August 2002 Flooding in Central Europe, J.
846 Hydrometeorol., 5, 656-678, 2004.



- 847 Stohl, A., James, P.: A Lagrangian analysis of the atmospheric branch of the global
848 water cycle. II. Moisture transports between Earth's ocean basins and river
849 catchments, *J. Hydrometeorol.*, 6, 961–984, 2005.
- 850 Trenberth, K.E., Fasullo, J., Smith, L.: Trends and variability in column-integrated
851 atmospheric water vapor, *Climate Dynamics*, 24, 741–758, 2005.
- 852 Trenberth, K.E., Smith, L., Qian, T., Dai, A., Fasullo, J.: Estimates of the global water
853 budget and its annual cycle using observational and model data, *J.*
854 *Hydrometeorol.*, 8, 758–769, 2007.
- 855 Van Der Ent, R.J., Savenije, H.H.G., Schaefli, B., Steele-Dunne, S.C. Origin and
856 fate of atmospheric moisture over continents, *Water Resources Research*, 46,
857 W09525, 2010.
- 858 Van Wijngaarden, W.A., Vincent, L.A.: Trends in relative humidity in Canada from
859 1953–2003, *Bulletin of the American Meteorological Society*, 4633–4636, 2004.
- 860 Vázquez, M., Nieto, R., Drumond, A., Gimeno, L.: Moisture transport into the Arctic:
861 Source-receptor relationships and the roles of atmospheric circulation and
862 evaporation, *Journal of Geophysical Research: Atmospheres*, 121, 493–509,
863 2016.
- 864 Vicente-Serrano, S.M., Azorin-Molina, C., Sanchez-Lorenzo, A., Revuelto, J., Morán-
865 Tejada, E., López-Moreno, J.I., Espejo, F.: Sensitivity of reference
866 evapotranspiration to changes in meteorological parameters in Spain (1961–
867 2011), *Water Resources Research*, 50, 8458–8480, 2014a.
- 868 Vicente-Serrano, S.M., Azorin-Molina, C., Sanchez-Lorenzo, A., Morán-Tejada, E.,
869 Lorenzo-Lacruz, J., Revuelto, J., López-Moreno, J.I., Espejo, F.: Temporal
870 evolution of surface humidity in Spain: recent trends and possible physical
871 mechanisms. *Climate Dynamics*, 42, 2655–2674, 2014b.
- 872 Vicente-Serrano, S.M., Azorin-Molina, C., Sanchez-Lorenzo, A., El Kenawy, A.,
873 Martín-Hernández, N., Peña-Gallardo, M., Beguería, S., Tomas-Burguera, M.:
874 Recent changes and drivers of the atmospheric evaporative demand in the
875 Canary Islands. *Hydrology and Earth System Science*, 20, 3393–3410, 2016.
- 876 Vincent, L.A., van Wijngaarden, W.A., Hopkinson, R.: Surface temperature and
877 humidity trends in Canada for 1953–2005, *Journal of Climate*, 20, 5100–5113,
878 2007.
- 879 Wang, K., Dickinson, R.E.: A review of global terrestrial evapotranspiration:
880 observation, modeling, climatology, and climatic variability, *Rev. Geophys.*, 50,
881 2012.
- 882 Willett, K.M., Jones, P.D., Gillett, N.P., Thorne, P.W.: Recent changes in surface
883 humidity: Development of the HadCRUH dataset, *Journal of Climate*, 21, 5364–
884 5383, 2008.
- 885 Willett, K.M., Dunn, R.J.H., Thorne, P.W., Bell, S., de Podesta, M., Parker, D.E., Jones,
886 P.D., Williams Jr., C.N.: HadISDH land surface multi-variable humidity and
887 temperature record for climate monitoring, *Clim. Past*, 10, 1983–2006, 2014.
- 888 Wright, J.S., Sobel, A., Galewsky, J.: Diagnosis of relative humidity changes in a
889 warmer climate, *J. Clim.*, 23, 4556–4569, 2010.
- 890 Yu, L.: Global variations in oceanic evaporation (1958–2005): The role of the changing
891 wind speed. *J. Climate*, 20, 5376–5390, 2007.
- 892 Yu, L., Jin, X., Weller, R.A.: Multidecade Global Flux Datasets from the Objectively
893 Analyzed Air-sea Fluxes (OAFlux) Project: Latent and sensible heat fluxes,
894 ocean evaporation, and related surface meteorological variables. Woods Hole
895 Oceanographic Institution, OAFlux Project Technical Report. OA-2008-01,
896 64pp. Woods Hole. Massachusetts. 2008.



- 897 Yue, S., Wang, C.: The Mann-Kendall Test Modified by Effective Sample Size to
898 Detect Trend in Serially Correlated Hydrological Series, *Water Resour.*
899 *Manage.*, 18, 201–218, 2004.
- 900 Zhang, X., Harvey, K. D., Hogg, W. D., and Yuzyk, T. R.: Trends in Canadian
901 streamflow, *Water Resour. Res.*, 37, 987–998, 2001.
- 902 Zhang, L., Wu, L., Gan, B.: Modes and mechanisms of global water vapor variability
903 over the twentieth century, *Journal of Climate*, 26, 5578–5593, 2013.
- 904 Zongxing, L., Qi, F., Wei, L., Tingting, W., Yan, G., Yamin, W., Aifang, C., Jianguo,
905 L., Li, L.: Spatial and temporal trend of potential evapotranspiration and related
906 driving forces in Southwestern China, during 1961–2009, *Quaternary*
907 *International*, 336, 127–144, 2014.
- 908
909
910
911
912
913

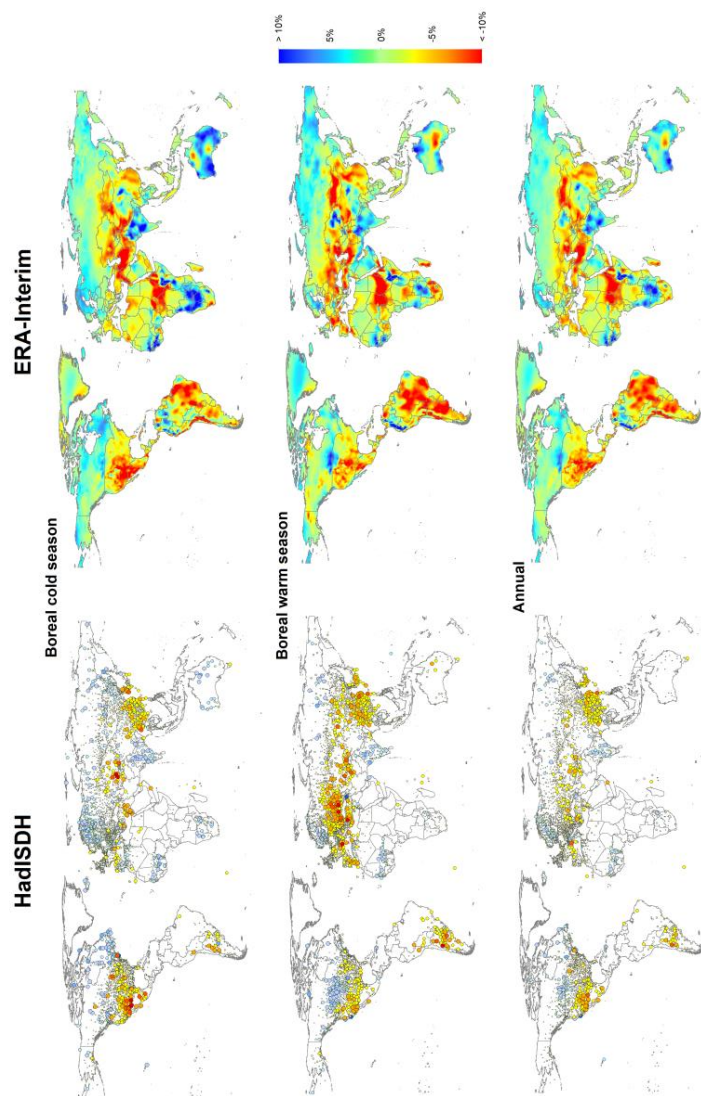


Figure 1. Spatial distribution of the magnitude of change of RH (% per decade) over the period 1979-2014 from HadISDH (left) and ERA-Interim dataset (right). Results are provided for the boreal cold (October-March) and warm (April-September) seasons and annually.

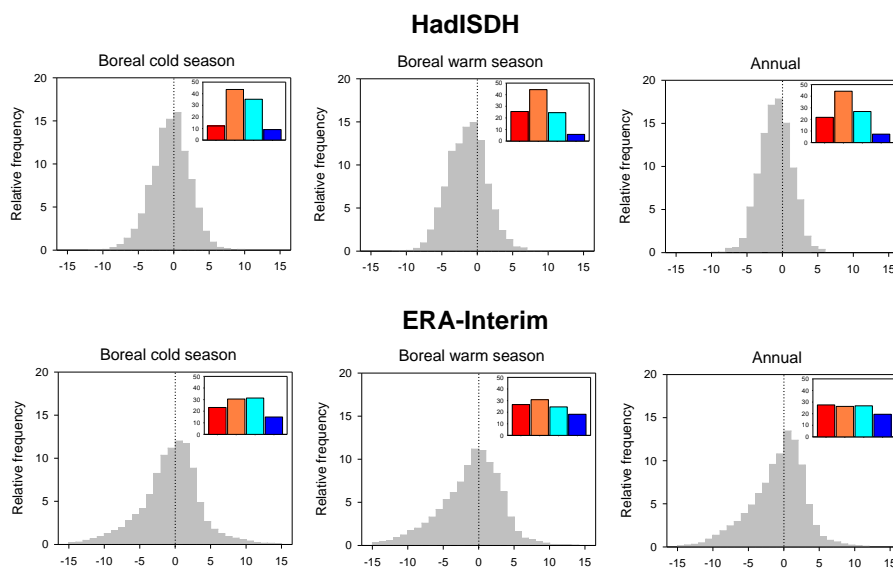


Figure 2: Relative frequencies (%) of the RH magnitude of change in the HadISDH and ERA-Interim datasets. Color bar plots represent the percentage of stations (from HadISDH) and world regions (from ERA-Interim) with positive and significant ($p < 0.05$) trends (blue), positive insignificant trends (cyan), negative insignificant trends (orange) and negative and significant trends (red).

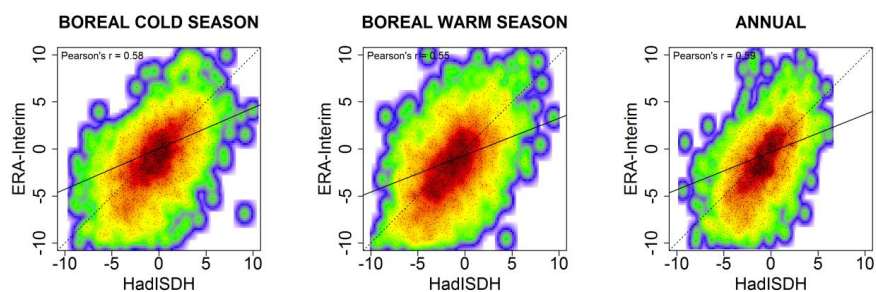


Figure 3: Scatterplots showing the global relationship between the magnitude of change in RH with HadISDH stations and ERA-Interim dataset at the seasonal and annual scales. Colors represent the density of points, with red color showing the highest density of points.

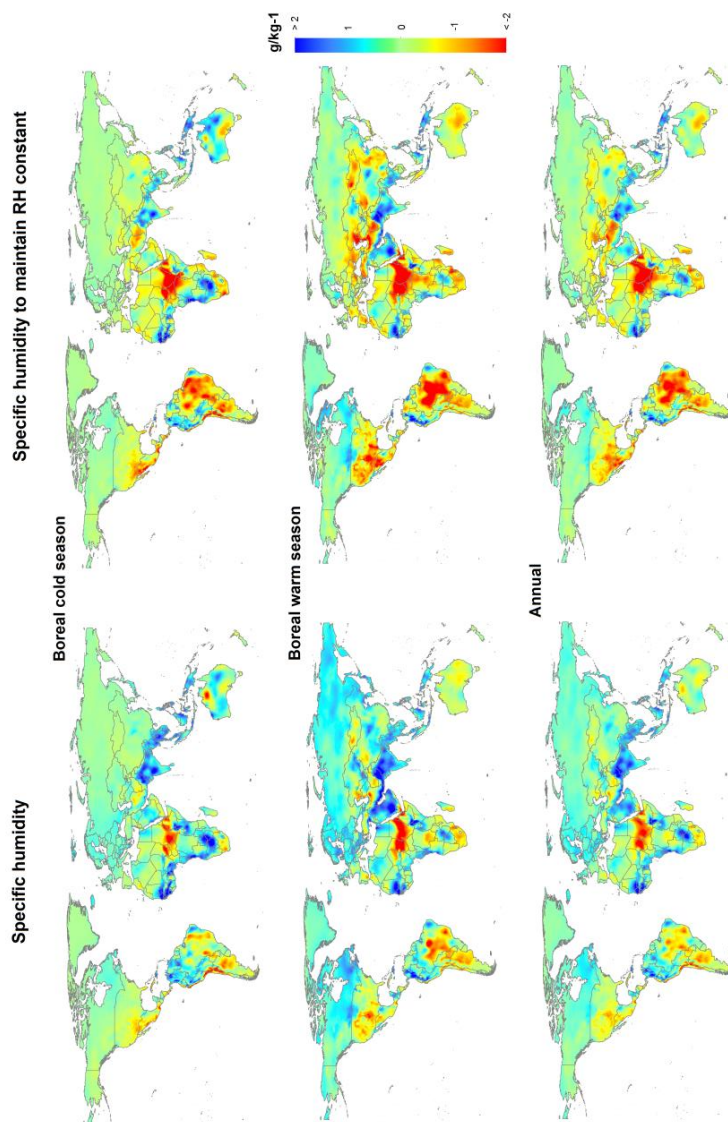


Figure 4: Spatial distribution of the seasonal and annual magnitudes of change in specific humidity (g/kg^{-1}) (left) and the deficit/surplus of specific humidity to maintain the RH constant with the levels of 1979 according to the land air temperature evolution (from the CRU TS v.3.23 dataset) for 1979-2014.

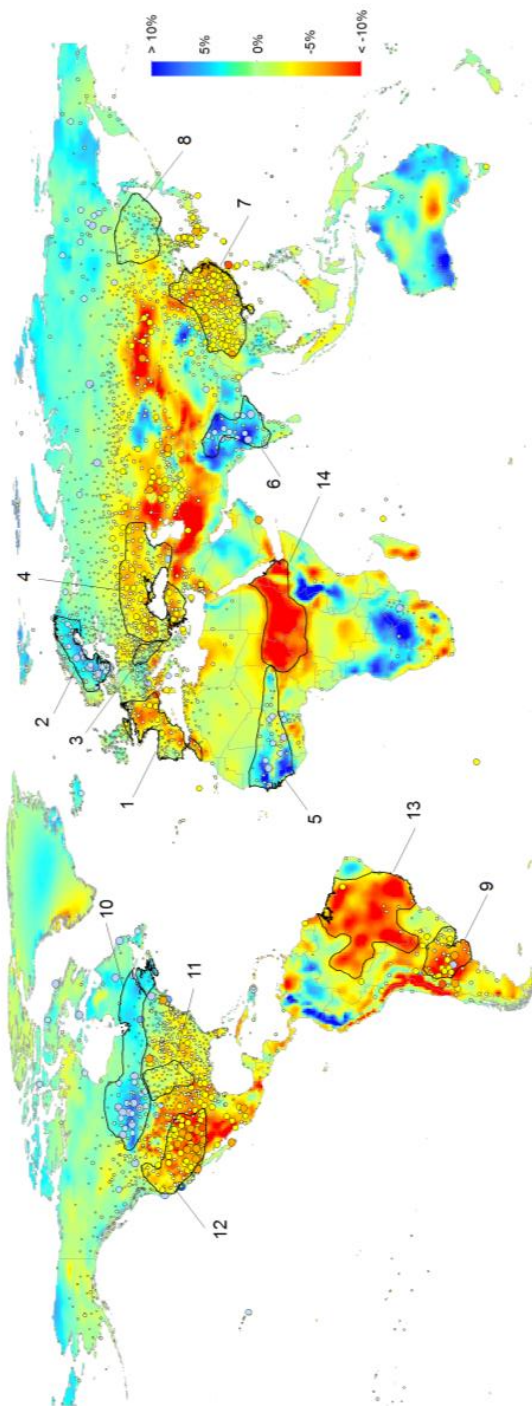


Figure 5: Distribution of the 14 world regions, with high consistency in RH trends between the HadISDH and the ERA-Interim datasets. These regions were selected for the identification of the oceanic and land humidity sources by means of the FLEXPART scheme.

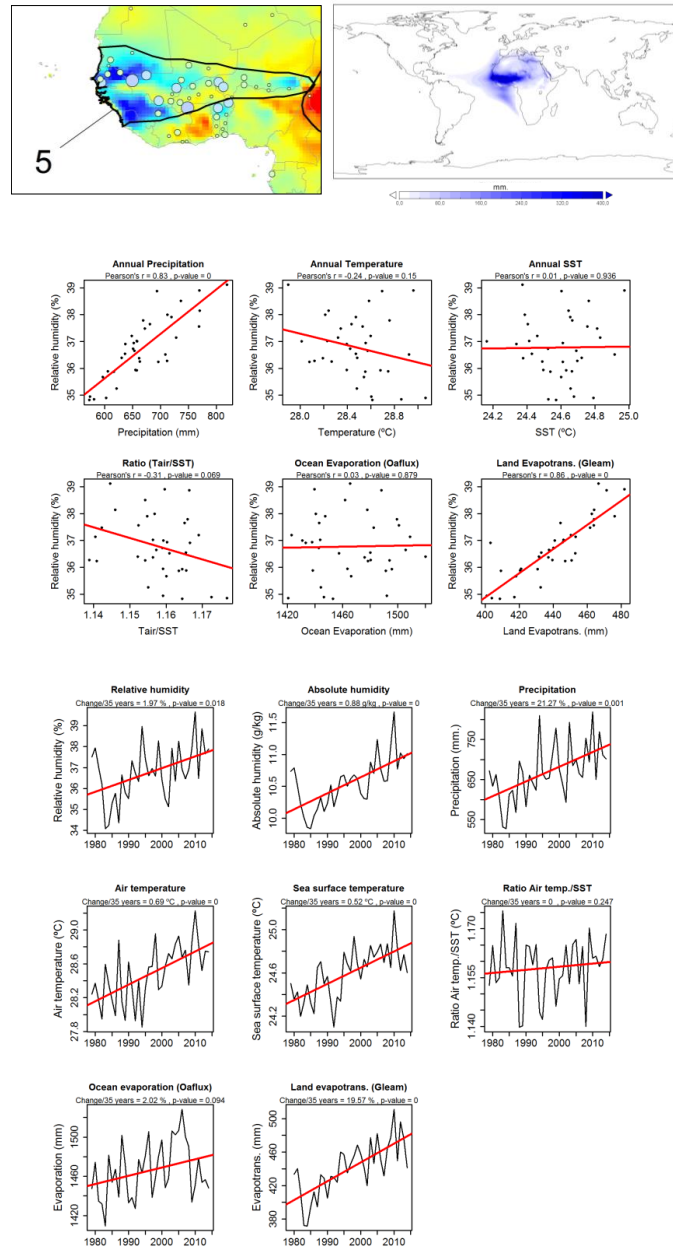


Figure 6: Top left: Annual RH humidity trends in the West Sahel (region 6), Top right: average $(E-P) > 0$ at the annual scale to identify the main humidity sources in the region (mm year^{-1}). Center: Relationship between the de-trended annual RH and the de-trended annual variables for 1979-2014. Bottom: Annual evolution of the different variables corresponding to the West Sahel region. The magnitude of change and signification of the trend is indicated for each variable.

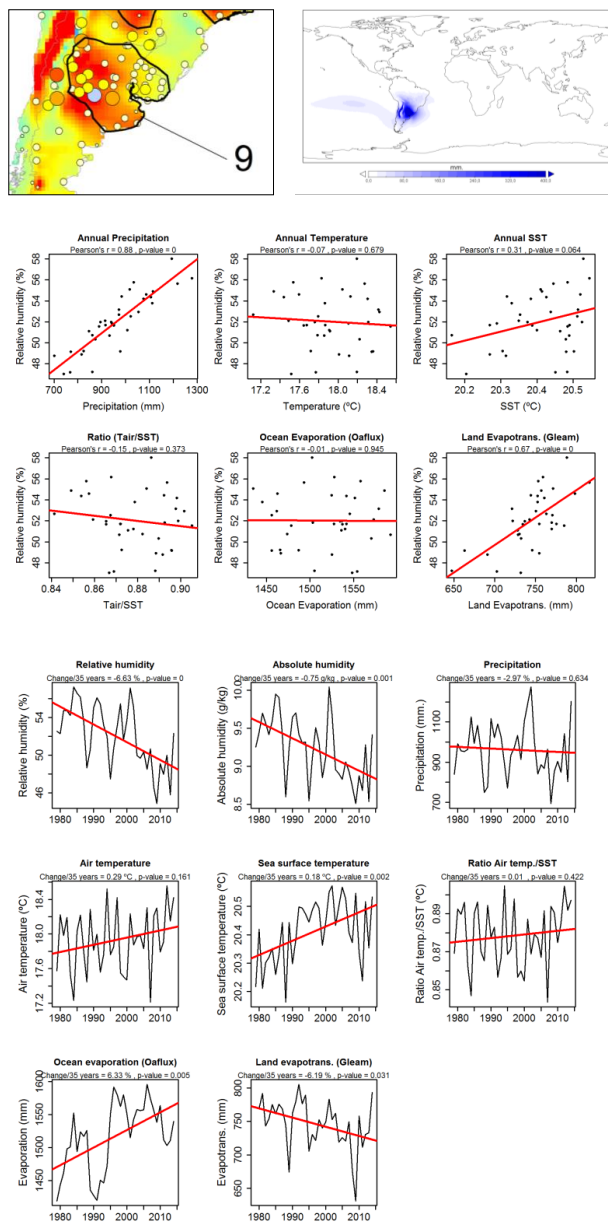


Figure 7: The same as Fig. 6 but for La Plata (region 9).

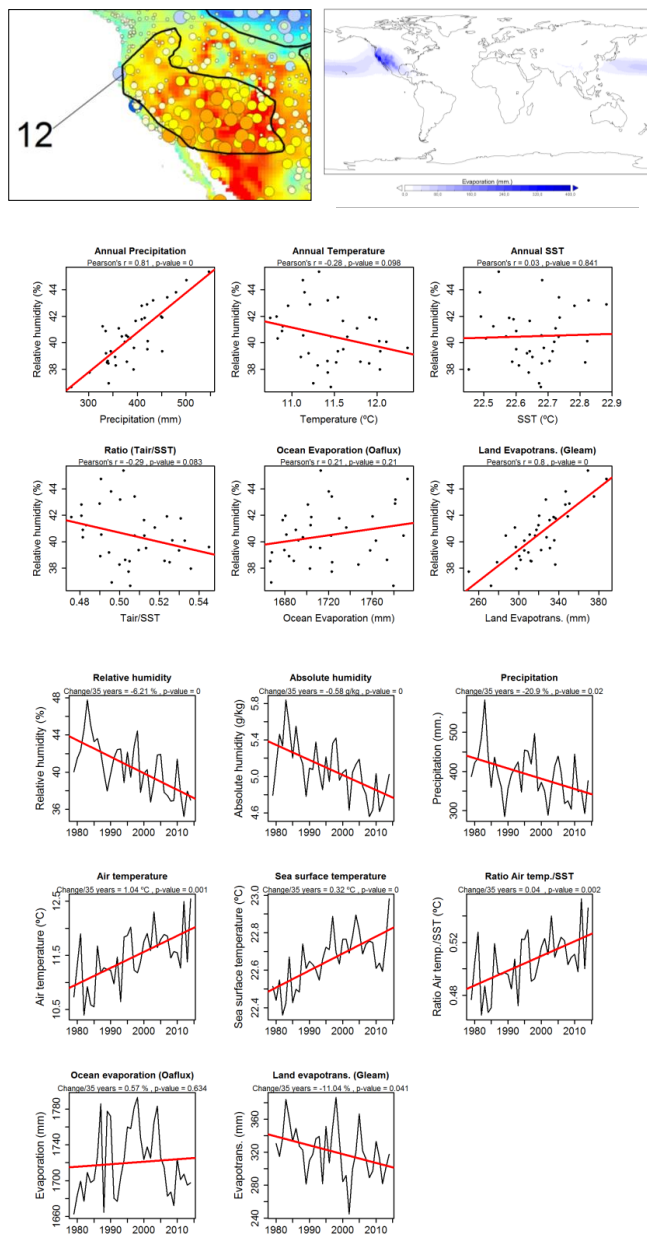


Figure 8: The same as Fig. 6 but for West North America (region 12).

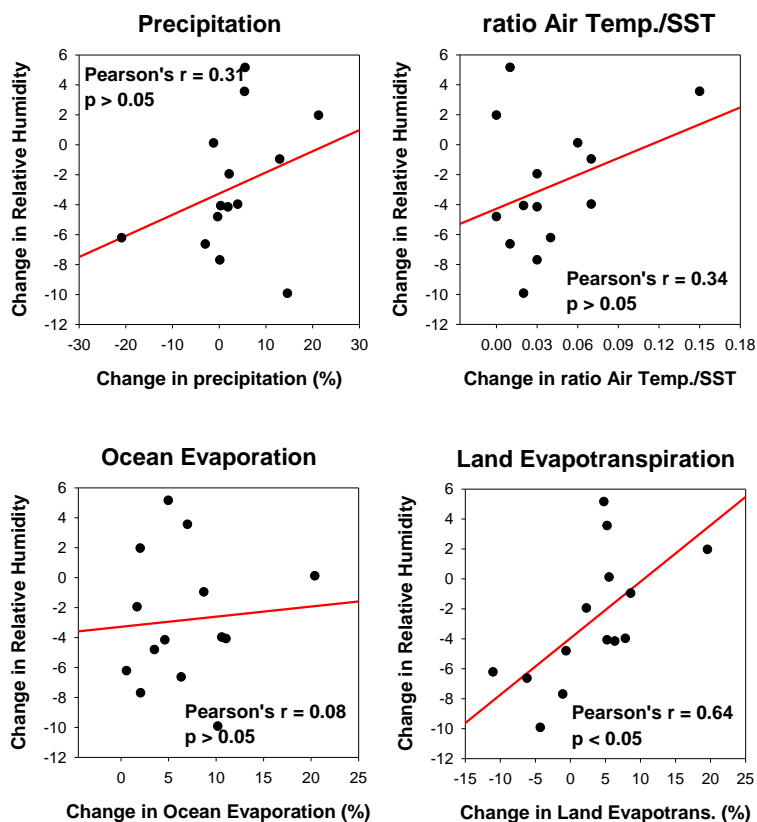


Figure 9: Relationship between the average annual magnitude of change in RH identified in each one of the 14 analyzed regions and the annual magnitude of change in precipitation, the ratio between air temperature/SST, oceanic evaporation and land evapotranspiration.

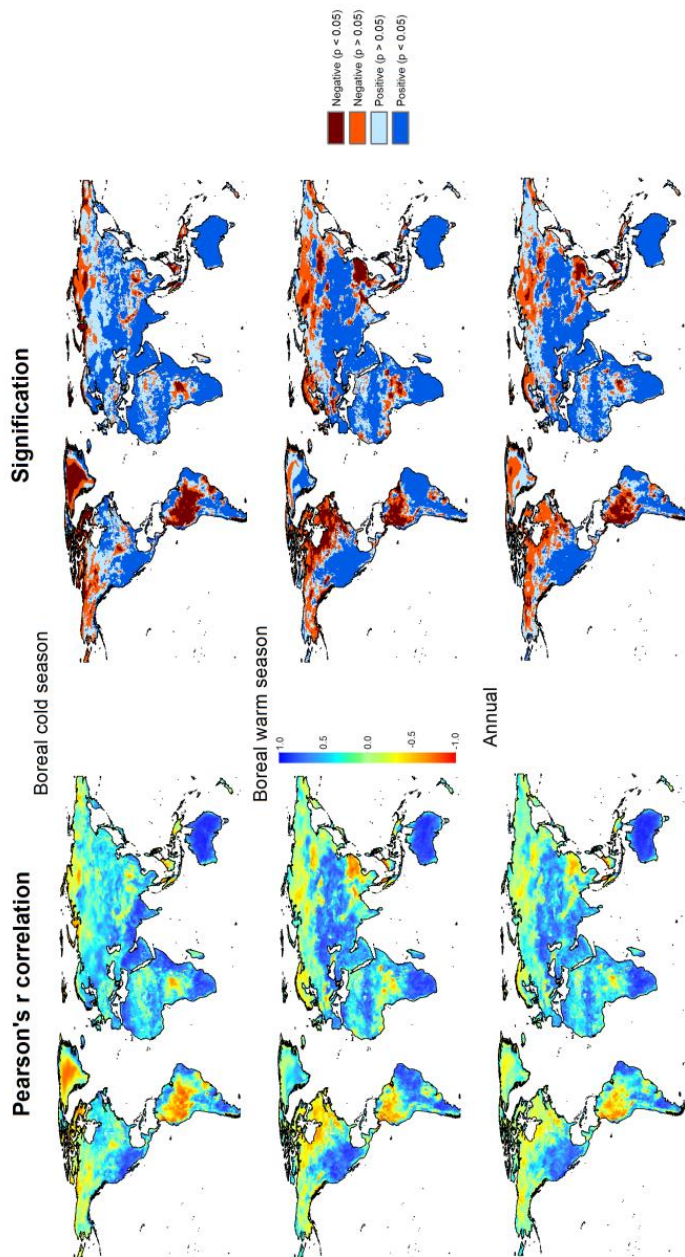


Figure 10: Spatial distribution of the Pearson's r correlations between the detrended RH and land evapotranspiration series at the annual and seasonal time scales. The signification of the correlations is also shown.

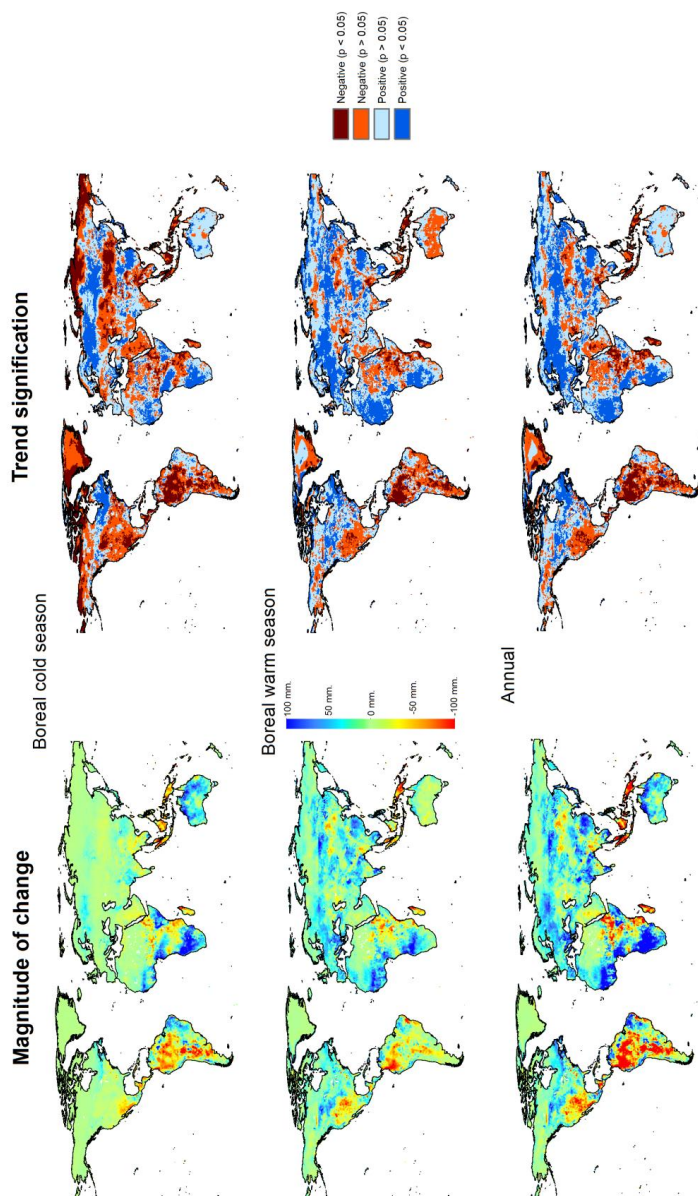


Figure 11: Spatial distribution of the magnitude of change in the annual and seasonal land evapotranspiration (1979-2014) and statistical significance of trends.

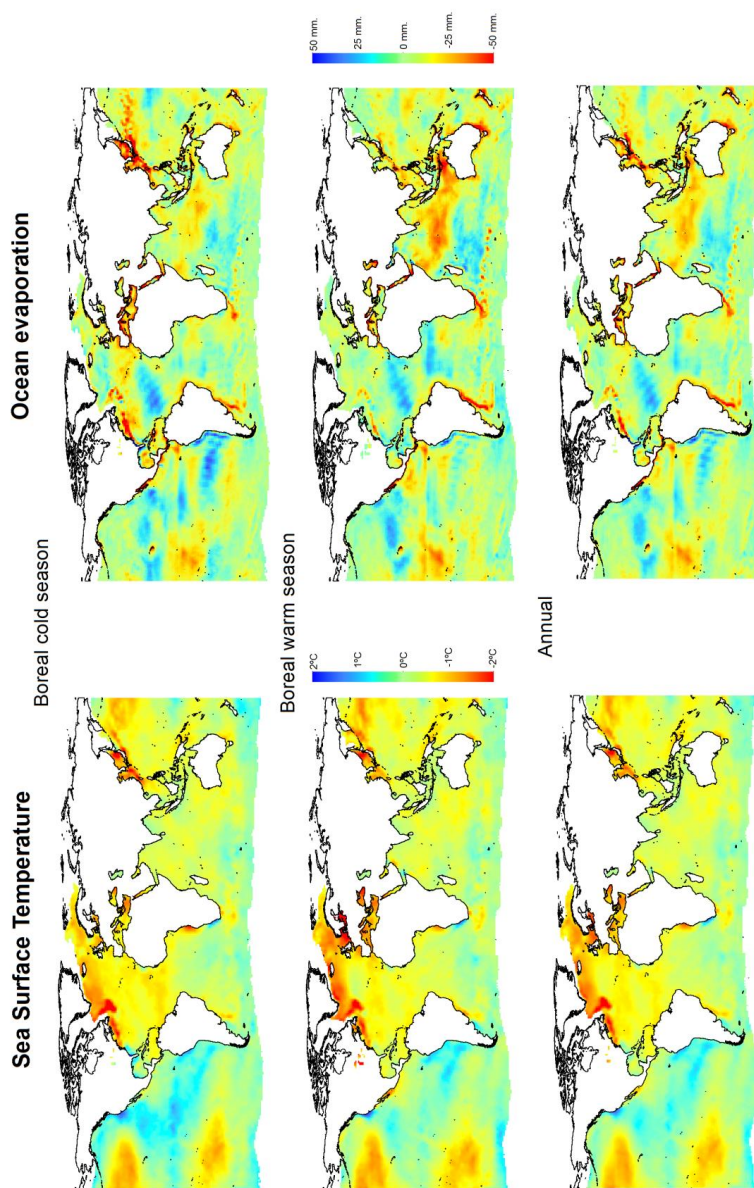


Figure 12: Annual and seasonal magnitude of change of SST and OAFLEX oceanic evaporation for 1979-2014.